Available online at www.sciencedirect.com

ScienceDirect

Procedia Structural Integrity 28 (2020) 1106–1115

Structural Integrity Procedia

www.elsevier.com/locate/procedia

1st Virtual European Conference on Fracture

Mixed-mode evaluation of ductile adhesive joints by the single-leg bending test

J.P.S.M.B. Ribeiro[a], Raul D.S.G. Campilho[a,b,*], R.J.B. Rocha[a,b]

[a]*School of Engineering, Polytechnic of Porto, ISEP-IPP, Rua Dr. António Bernardino de Almeida, 431, 4200-072, Portugal*
[b]*Institute of Science and Innovation in Mechanical and Industrial Engineering, Rua Dr. Roberto Frias, 4200-465, Portugal.*

Abstract

In the design of adhesive structures, it is extremely important to accurately predict their strength and fracture properties (critical strain energy release rate in tension, G_{IC}, and shear, G_{IIC}). In most cases, the loads occur in mixed-mode (tension plus shear). Thus, it is of great importance the perception of fracture in these conditions, namely of the strain energy release rates in tension, G_I, and shear, G_{II}, relative to different crack propagation criteria or fracture envelopes. This comparison allows to determine the most suitable energetic propagation criterion to be used in cohesive zone models (CZM). The main objective of this work is to verify, by CZM, which is the power law parameter (α) that best suits the energetic crack propagation criterion for CZM modelling, using single-lap joints (SLJ) and double-lap joints (DLJ) with aluminium adherends and bonded with a ductile adhesive. With this purpose, numerical simulations of the SLJ and DLJ are carried out, and the maximum load (P_m) is compared with experiments. For the tested materials and geometries, the energetic criterion resulting from the experimental work provided matching numerical results and, thus, the fracture envelope was validated.

Keywords: Bonded joint; Finite Element analysis; Cohesive zone models; Mixed-mode fracture; Fracture envelope.

1. Introduction

In the present time, adhesively-bonded joints are used in numerous industrial fields due to several advantages over other joining methods, e.g. welding, riveting and fastening. In fact, from a simple shoe to a space shuttle, adhesives

* Corresponding author. Tel.: +351 939526892; fax: +351 228321159.
E-mail address: raulcampilho@gmail.com (R.D.S.G. Campilho).

2452-3216
10.1016/j.prostr.2020.11.125

are employed to bond similar and dissimilar materials (da Silva et al. 2011). This technique's advantages include preserving the integrity of the parent materials, since it avoids any structural damage (i.e. no holes or heating), thus providing a better stress distribution along the bonded area (Petrie 1999). Additionally, improved strength-weight and cost-effectiveness ratios can be attained, which are highly relevant for the industry and designers in the pursuit of better products (da Silva et al. 2011). Few other benefits such as flexible gap filing, noise and vibration damping, excellent insulation and improved aesthetics are inherent to this method. Nevertheless, some drawbacks still persist, such as the requirement of a surface treatment, disassembly issues without causing damage, low resistance to temperature and humidity, and joint design orientated towards the elimination of peel stresses (Adams 2005). A number of joint architectures is available depending on the different applied loads. Among those, the SLJ is the most studied one. In fact, SLJ are simple to manufacture, although the adherends are not aligned, causing major peel (σ_y) stresses at the overlap ends (Petrie 1999). The DLJ, slightly more difficult to produce, manages to decrease the bending moment due to its balanced design, thus reducing both σ_y and shear (τ_{xy}) stresses. Despite that, internal bending moments may occur, triggering σ_y stresses at the ends of the inner adherend. Moreover, one may find commonly other joint architectures, such as butt, strap, scarf, step, tubular and T-joints (Petrie 1999).

The development of trustworthy predictive methods is required for a widespread use of adhesively-bonded joints. Despite few analytical solutions being capable to quickly predict the joints' behaviour, the process could become extremely complex when composite adherends are used or in the presence of adhesives with high plasticity. The Finite Element (FE) method is capable to overcome such issues and is by far the most common technique used in bonded joints (He 2011). Several approaches were developed along the years, such as continuum mechanics, fracture and damage mechanics techniques. Later, during the sixties, Barenblatt (1959) and Dugdale (1960) proposed the concept of cohesive zone to describe damage under static loads. This method simulates the damage along a predefined crack path thru the establishment of a load-displacement (P-δ) correlation, known as traction-separation law. These laws associate the cohesive tractions (t_n for tension and t_s for shear) with the relative displacements (δ_n for tension and δ_s for shear). To obtain good agreement between the predicted strength and the experiments, a truthful estimation of the cohesive strengths in tension and in shear (t_n^0 and t_s^0, respectively), and G_{IC} and G_{IIC} is essential. Usually, an adhesive joint may be put under σ_y or τ_{xy} stresses, although in most cases it is subjected simultaneously to both, thereby creating a mixed-mode loading.

Several tensile fracture characterization tests to evaluate G_{IC} are available, such as the Double-Cantilever Beam (DCB), the Tapered Double-Cantilever Beam (TDCB), the Compact Tension and the Single-Edge Notched Bending. The DCB test became the most used, being supported by several standards (e.g. the ASTM D3433), providing guiding processes for the experiments and data reduction. This test requires an initial crack introduced during the fabrication process at the adhesive-free edge of the specimen, which will propagate by applying an opening load at the specimen's edge. The R-curve plots the G_I against the crack length (a). In theory, this curve provides a perfectly horizontal G_I-a curve during damage growth, whose steady-state value gives the measurement of G_{IC}. Shear fracture testing is considerably more complex and is yet to be standardized (Sistaninia and Sistaninia 2015). Nonetheless, several different tests have been proposed: End-Notched Flexure (ENF), 4-Point End-Notched Flexure and End-Loaded Split. Among those, the most commonly used is the ENF, which presents a simple three-point bending setup and reliable data reduction methods. It requires a pre-cracked specimen and a constant measurement of P, δ and a. Since adhesive joints are typically subjected to mixed-mode, few tests are also available to evaluate the mixed-mode strain energy release rate (G), such as the Asymmetric Double-Cantilever Beam, the Mixed-Mode Flexure, the Mixed-Mode Bending (MMB) and the Single-Leg Bending (SLB). The MMB test is the only standardized test available to estimate G of composites, referred in ASTM D6671. A combination of the DCB and ENF is the basis of the MMB test (Choupani 2008), and allows to change the mixed-mode ratio almost without limit between the pure mode I and pure mode II loading conditions. Hence, it provides a complete understanding of the joints' fracture behaviour under different loadings, known as fracture envelope. The SLB test is simpler than the MMB as it does not require special jigs. However, is more limited with respect to the change of the mixed-mode ratio.

Rodrigues et al. (2017) determined the fracture envelope of an aluminium adhesive bonded joint in dry and wet conditions, enabling to predict the humidity effect on G. After assessing the adhesive moisture absorption capability, DCB and ENF fracture tests were performed for mode I and II, respectively. For the mixed-mode test, an apparatus was used that allows to test within a range of mode combinations between pure-modes I and II. The dry and wet fracture envelopes showed the ageing effect on the P_m and P-δ curves. Moreover, the applied methodology enabled

obtaining the full fracture envelope with a linear correlation between the pure and mixed-mode data points. Nunes and Campilho (2018) estimated the fracture envelope of joints bonded with three adhesives with different ductility using the Asymmetric Tapered Double-Cantilever Beam (ATDCB) mixed-mode test. Pure-mode TDCB tests and the Corrected Beam Theory were used to assess G_{IC}, and the ENF test together with the Compliance-Based Beam Method (CBBM) served to estimate G_{IIC}. CZM laws were built based on a triangular law and the power law mixed-mode growth criterion, and the respective numerical results were compared with the experiments. This enabled to validate the CZM laws and the mixed-mode propagation criterion of each adhesive. Some inconsistencies were detected in the stiffness and P_m of the most ductile adhesive, since the triangular law was not suitable to capture the plasticity inherent to theses adhesives (Rocha and Campilho 2018). However, the authors manage to prove that the data reduction method used for the ATDCB specimens is accurate and quick.

The main objective of this work is to verify, by CZM, which is the α value that best suits the energetic crack propagation criterion for CZM modelling, using SLJ and DLJ with aluminium adherends and bonded with the Araldite® 2015 adhesive. With this purpose, numerical simulations of the SLJ and DLJ are carried out, and P_m is compared with experiments.

2. Experimental details

2.1. Joint materials (fracture tests and lap joints)

The DCB, ENF and SLB adherends, used to build the fracture envelopes of the adhesives, were manufactured from CFRP plates. The composite plates were fabricated using 20 plies with 0.15 mm thickness each, stacked by hand-lay-up using unidirectional layers. The SEAL® Texipreg HS 160 RM pre-preg was used in this process. The curing process took 1 hour to accomplished and was carried out in a hot-plates press under a temperature and pressure of 130ºC and 2 bar, respectively. The elastic-orthotropic properties of an CFRP unidirectional layer fabricated under similar conditions can be found in the work from Ribeiro et al. (2016). The SLJ and DLJ tested in this work for validation purposes were fabricated from an aluminium alloy sheet metal with reference AW6082-T651. This alloy presents several important features, which were relevant during the material selection, such as the good mechanical properties and the wide field of structural applications in the laminated form. The ductile adhesive Araldite® 2015 was used to bond the adherends. The mechanical and fracture properties that were evaluated in previous works (Campilho et al. 2011, Campilho et al. 2013), are described in Table 1.

Table 1. Mechanical and fracture properties of the adhesive Araldite® 2015 (Campilho et al. 2011, Campilho et al. 2013).

Property	2015
Young's modulus, E [GPa]	1.85±0.21
Poisson's ratio, ν	0.33 [a]
Tensile yield stress, σ_y [MPa]	12.63±0.61
Tensile strength, σ_f [MPa]	21.63±1.61
Tensile failure strain, ε_f [%]	4.77±0.15
Shear modulus, G [GPa]	0.70 [b]
Shear yield stress, τ_y [MPa]	14.6±1.3
Shear strength, τ_f [MPa]	17.9±1.8
Shear failure strain, γ_f [%]	43.9±3.4
Toughness in tension, G_{IC} [N/mm]	0.43±0.02
Toughness in shear, G_{IIC} [N/mm]	4.70±0.34

[a] manufacturer's data

[b] estimated from the Hooke's law using E and ν

2.2. Joint dimensions, fabrication and testing

Fig. 1 illustrates the dimensions and geometry of DCB, ENF and SLB specimens, whereas Fig. 2 represents the geometry and dimensions of the SLJ and DLJ.

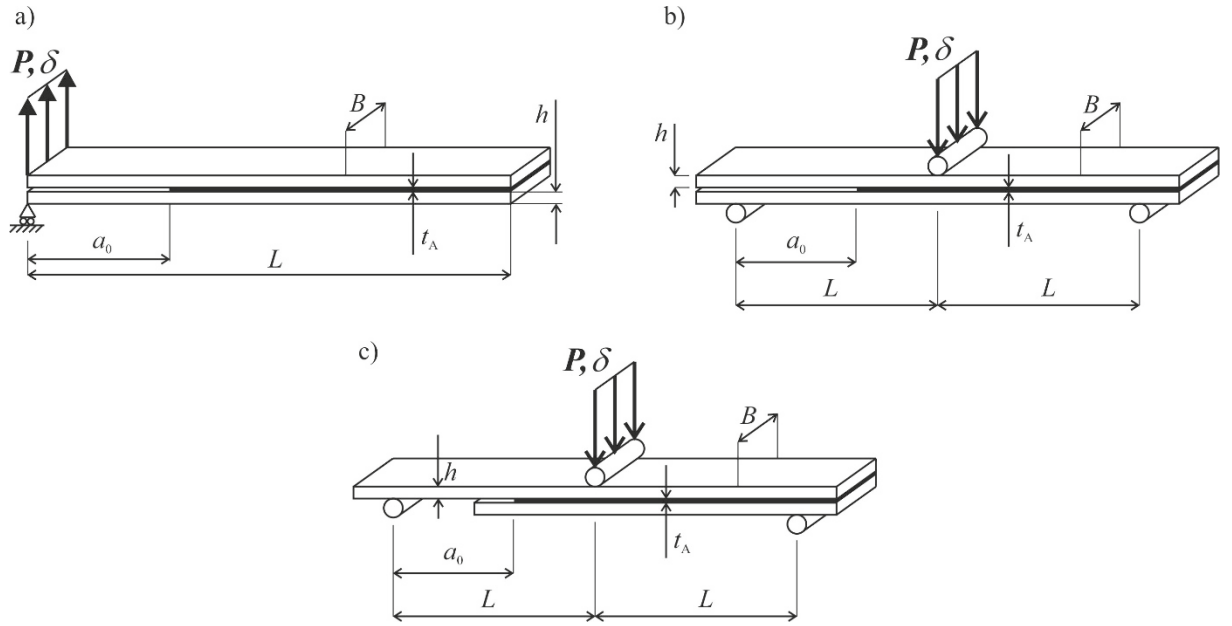

Fig. 1. Geometry and dimensions of the DCB (a), ENF (b) and SLB specimens (c).

The specimens' dimensions were as follows next (in mm): total length or mid-span L=180 (SLJ and DLJ), L=140 (DCB) or L=100 mm (ENF and SLB), initial crack length a_0≈40 mm (DCB) or a_0≈60 mm (ENF and SLB), adherends' thickness h=3, adhesive thickness t_A=0.2, joints' width B=25 and overlap length L_O=12.5, 25, 37.5 and 50 (SLJ and DLJ only). In the present work, the DLJ were fabricated with equal h in the middle and outside adherends, which is not consistent with the existence of cross-section balanced adherends. This occurs if the middle adherend has twice h than the outer adherends. However, this was a testing choice that does not compromise the fracture envelopes' validation purpose that this work aims to. Six specimens for each condition were tested for the fracture tests, while five specimens were evaluated for the lap geometries.

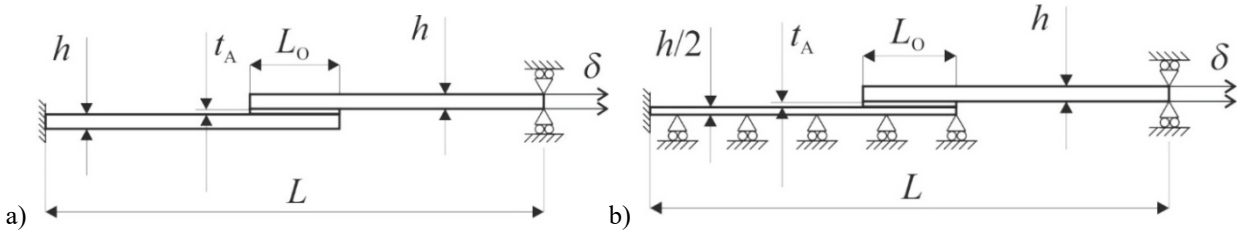

Fig. 2. Geometry and dimensions of the single (a) and double-lap joint (b).

For both CFRP and aluminium adherends, the surface preparation prior to bonding was similar: the bonding surfaces were manually abraded using a fine sandpaper to completely remove the shiny surface or aluminium oxide layer, respectively, followed by cleaning and degreasing with acetone. For all tests, and to promote a reliable and dimensionally accurate bonding, the joined parts were placed in a steel mould during the curing process. To guarantee a correct value of t_A, for the DCB, ENF and SLB specimens, calibrated metallic spacers were placed between the superior and inferior adherends. These specimens shared the same pre-crack induction method, which consisted in the placement of spacers, in which the crack-tip spacer had a centred sharp razor blade. Nonetheless, to avoid any blunting effects, in each specimen the crack was manually propagated for a length between 1 and 3 mm, and only after the a_0

measurement took place. In the case of the SLJ and DLJ, t_A was achieved using metallic blocks that were placed in the mould. Regardless the joint type, after pouring the adhesive in one of the adherends, the two adherends were joined and pressured until there was contact with the spacers. This process had to be repeated one more time for the DLJ. Then, the one week curing process initiated. After curing, the spacers or blocks were removed, and the excess adhesive was removed using milling techniques. To allow the measurement of a, one side of the DCB, ENF and SLB joints was painted with a brittle white paint and a numbered scale was glued on that side to allow tracking crack propagation. All specimens were tested in an electro-mechanical testing machine Shimadzu AG-X 100 equipped with a 100 kN load cell. The fracture tests were documented by taking pictures with 5 s intervals, using a digital 18 MPixel camera with no zoom and placed at a focal distance of 100 mm. The DCB, SLJ and DLJ specimens were tested in conventional tension, while the ENF and SLB specimens were tested using a three-point bending setup. All tests were carried at room temperature and 1 mm/min of velocity. The manual a measurement in the DCB, ENF and SLB tests was done by approximating the crack tip to the nearest 1/8 of mm in the scale, which was made possible by the resolution of the images (0.02 mm/pixel).

2.3. Fracture toughness estimation

Typically, failure in adhesive bonds takes place under mixed-mode due to the different properties of the joints' components, the applied load and joint architecture, which demands the knowledge of both G_{IC} and G_{IIC}, and also the use of mixed-mode criteria (Nunes and Campilho 2018). In this work, the CBBM data reduction method was selected to estimate G_{IC} and G_{IIC} from the DCB and ENF tests, respectively, and G_I and G_{II} from the SLB tests. The CBBM provides the fracture measurements only from the experimental compliance (C) measured during the tests (de Moura et al. 2009). This method procedure includes an equivalent crack length (a_{eq}), which is defined from the P-δ curve. Moreover, it accounts for the Fracture Process Zone (FPZ), which generates around the crack tip due to the materials' plasticity, otherwise neglected in the analysis when considering the measured value a. For the DCB specimen, G_{IC} is calculated as

$$G_{IC} = \frac{6P^2}{B^2 h}\left(\frac{2{a_{eq}}^2}{h^2 E_f} + \frac{1}{5G_{xy}}\right), \tag{1}$$

where E_f is a corrected flexural modulus to account for stress concentrations at the crack tip and stiffness inconsistency between specimens, and G_{xy} is the shear modulus of the adherends. Full derivation can be found in the study of Constante et al. (2015). Applied to the ENF test, G_{IIC} can be obtained by the following expression

$$G_{IIC} = \frac{9P^2{a_{eq}}^2}{16B^2 E_f h^3}. \tag{2}$$

A detailed description of the method can be found in reference (de Moura et al. 2009). The CBBM applied to the SLB specimens is based on the beam theory of Szekrényes and Uj (2004). Application of the Irwin-Kies expression gives the total energy release rate (G_T) which, after equation splitting according to Szekrényes and Uj (2004), provides G_I and G_{II}

$$G_I = \frac{12P^2{a_{eq}}^2}{16B^2 E_f h^3} + \frac{3P^2}{10G_{xy}B^2 h} \text{ and } G_{II} = \frac{9P^2{a_{eq}}^2}{16B^2 E_f h^3}. \tag{3}$$

3. Numerical details

3.1. Model's construction

Numerical simulations were undertaken in Abaqus®, in order to validate the experimentally estimated fracture envelopes further in this work. The two-dimensional models included geometrical non-linearities. The models were based on plane-strain elements (CPE4 of Abaqus®) for the adherends with elastic-plastic continuum formulation and cohesive elements (COH2D4 of Abaqus®) for the adhesive layer. It should be stressed that, for all DLJ models, horizontal symmetry was applied to reduce the computational effort. The mesh refinement described next always assured mesh convergence. The elements' size at the adhesive layer's edges was 0.2 mm × 0.2 mm. For all the models, a total of 8 elements was considered in the adherends through-thickness, whereas between 40 and 160 solid elements were introduced length-wise in the adhesive layer length (between the smallest and largest L_O). To speed up the simulations, although without compromising the analysis results, the FE mesh was graded horizontally and vertically. All models were fixed at one edge while a vertical restraint and tensile displacement were applied at the opposite edge.

3.2. Mixed-mode triangular model

CZM are based on a relationship between stresses and relative displacements (in tension or shear) connecting paired nodes of cohesive elements (Fig. 3), to simulate the elastic behaviour up to t_n^0 in tension or t_s^0 in shear and subsequent softening, to model the degradation of material properties up to failure. The shape of the softening region can also be adjusted to conform to the behaviour of different materials or interfaces (Kafkalidis and Thouless 2002). The areas under the traction-separation laws in tension or shear are equalled to G_{IC} or G_{IIC}, by the respective order. Under pure loading, damage grows at a specific integration point when stresses are released in the respective damage law. Under a combined loading, stress and energetic criteria are often used to combine tension and shear (Feraren and Jensen 2004). The triangular law (Fig. 3) assumes an initial linear elastic behaviour followed by linear degradation. Elasticity is defined by a constitutive matrix (**K**) containing the stiffness parameters and relating stresses (***t***) and strains (***ε***) across the interface (Abaqus® 2013)

$$\boldsymbol{t} = \begin{Bmatrix} t_n \\ t_s \end{Bmatrix} = \begin{bmatrix} K_{nn} & K_{ns} \\ K_{ns} & K_{ss} \end{bmatrix} \cdot \begin{Bmatrix} \varepsilon_n \\ \varepsilon_s \end{Bmatrix} = \mathbf{K}\boldsymbol{\varepsilon}. \tag{4}$$

t_n and t_s are the current tensile and shear tractions, respectively, and and ε_n and ε_s the corresponding strains. A suitable approximation for thin adhesive layers is provided with $K_{nn}=E$, $K_{ss}=G_{xy}$ and $K_{ns}=0$ (Moreira and Campilho 2015). Damage initiation can be specified by different criteria. In this work, the quadratic nominal stress criterion was considered for the initiation of damage, already shown to give accurate results (Moreira and Campilho 2015) and expressed as (Abaqus® 2013)

$$\left\{ \frac{\langle t_n \rangle}{t_n^0} \right\}^2 + \left\{ \frac{t_s}{t_s^0} \right\}^2 = 1. \tag{5}$$

$\langle\ \rangle$ are the Macaulay brackets, emphasizing that a purely compressive stress state does not initiate damage. After the mixed-mode cohesive strength is attained (t_m^0 in Fig. 3) by the fulfilment of equation (5), the material stiffness is degraded. Complete separation is normally predicted by a linear power law form of the required energies for failure in the pure modes by considering the power law exponent α=1 (Abaqus® 2013)

$$\left(\frac{G_I}{G_{IC}} \right)^{\alpha} + \left(\frac{G_{II}}{G_{IIC}} \right)^{\alpha} = 1. \tag{6}$$

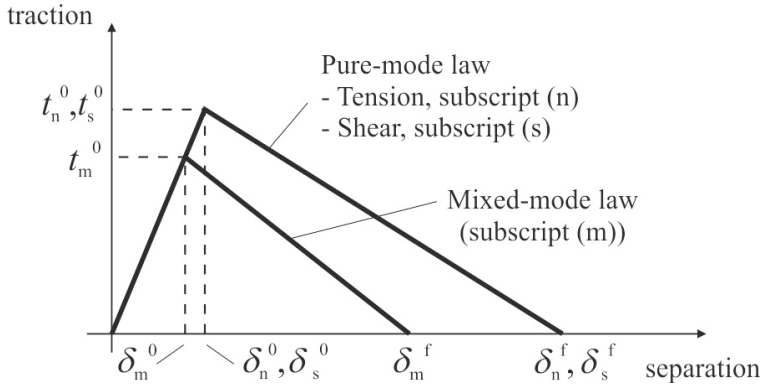

Fig. 3. Traction-separation law with linear softening law available in ABAQUS®.

4. Results

4.1. Fracture envelopes of the adhesives

4.1.1. G_{IC} and G_{IIC} calculation by the DCB and ENF tests

G_{IC} and G_{IIC} were calculated by the CBBM data reduction method using the DCB and ENF tests, respectively. The P-δ curves obtained for both tests were all consistent. All specimens suffered a gradual failure accompanied by a reduction of P. The R-curves depicted the expected steady-state crack growth for both loading modes, which represent the G_{IC} and G_{IIC} values. Nevertheless, crack propagation presented few oscillations mainly owing to small fabrication defects and imperfections, adhesive mixing variations and crack arrest phenomena. In the ENF test, G_{IIC} can be measured up to the crack reaching the proximity of the loading cylinder, because at this zone the almost pure-shear stress state is cancelled due to the compression effect. The average of the fracture toughness was 0.54 and 2.96 N/mm for G_{IC} and G_{IIC} respectively. deviation of all specimens bonded with the three adhesives. The highest standard deviation, normalized over the average fracture toughness, was 0.23% for the G_{IIC}, depicting the repeatability of the experimental tests. Comparing these values with the ones presented in Table 1, deviations of +25.6 and -37.1%, were found for G_{IC} and G_{IIC}, respectively. These differences are justified by the dependence of G_{IC} and G_{IIC} with the specimens' geometry, more specifically with h and t_A, given that these parameters influence FPZ' size in the vicinity of the crack tip (Pardoen et al. 2005).

4.1.2. G_{IC} and G_{IIC} calculation by the SLB test

The P-δ curves of the SLB specimens are depicted in Fig. 4 (a), showing an example of the repeatability between specimens.

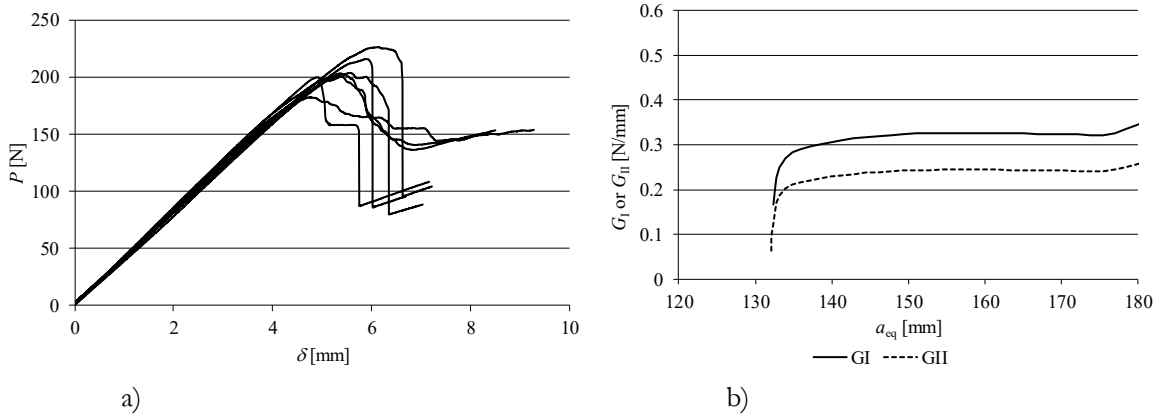

Fig. 4. P-δ curves (a) and experimental R-curves (b) from SLB specimens bonded with the Araldite® 2015.

Generally, a good reproducibility was found regarding the elastic stiffness (up to P_m). The crack growth behaviour was also similar. The ductility of the Araldite® 2015 led to a softening near P_m. Fig. 4 (b) shows the experimental R-curves where crack propagates at a fairly accurate steady-state value of G_I or G_{II} (for $140 \leq a_{eq} \leq 180$).

This constant crack growth region was the one considered to estimate both G_I or G_{II} values. In fact, when the adhesive FPZ spreads to the loading cylinder, the toughness artificially increases owing to compression effects.

4.1.3. Fracture envelope

The fracture envelope depicted in Fig. 5 was constructed from the mixed-mode results of the SLB tests and the pure-mode G_{IC} and G_{IIC} values, using the CBBM data reduction method. Four theoretical fracture envelopes are presented, by applying an energetic crack propagation criterion of the type of equation (6) with the exponents α=1/2, 1, 3/2 and 2. This will enable framing the behaviour of each adhesive in the most appropriate criterion. It was found some scatter in the experimental outcomes, even though this was still satisfactory. Actually, the deviation found for G_I and G_{II} was by 9.4 and 9.2%, respectively. The energetic propagation criterion with α=1/2 provides a good agreement to the behaviour of the Araldite® 2015.

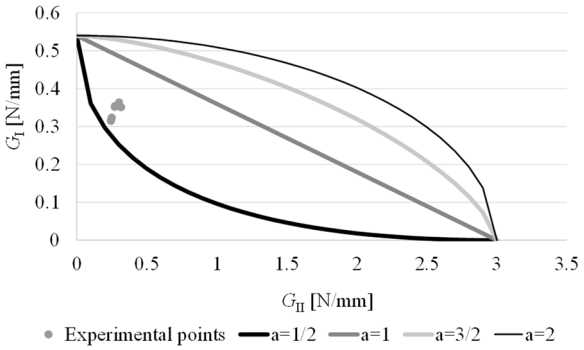

Fig. 5. Idealised fracture envelopes and experimental G_I/G_{II} data points for the adhesive Araldite® 2015.

4.2. Validation with lap geometries

4.2.1. Experimental testing

Fig. 6 provides the experimental P_m of the SLJ and DLJ bonded with the Araldite® 2015 as a function of L_O. Here, the values of E and G_{xy} have a major influence on the stress distributions and, thus, on P_m. Actually, Adams (2005) proved that joints with ductile adhesives undergo plasticity at the bond edges at the same time that the inner bond becomes increasingly loaded, which is usually linked to an increase in P_m.

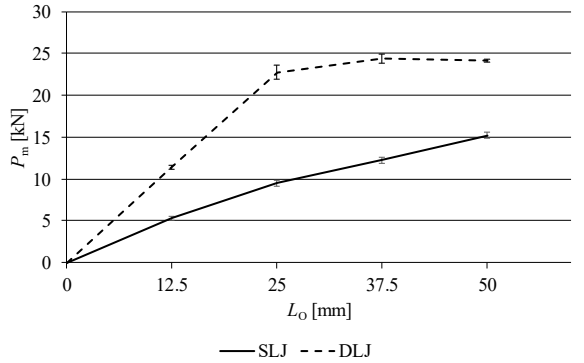

Fig. 6. Experimental P_m values for the SLJ and DLJ bonded with the Araldite® 2015.

On the one hand, observing the results for the SLJ (Fig. 6), P_m attained values of 5.3, 9.5, 12.2 and 15.2 kN, for L_O=12.5, 25, 37.5 and 50 mm, respectively. The strength improvement with L_O shows a linear trend up to L_O=50 mm. Actually, a P_m increase of 79.3% was found when L_O increases from 12.5 to 25 mm, 29.1% from 25 to 37.5 mm and 24.1% from 37.5 to 50 mm. On the other hand, for the DLJ, the P_m was by 11.4, 22.7, 24.4 and 24.1 kN, for L_O=12.5, 25, 37.5 and 50 mm, respectively. It is notorious that the strength increases with L_O up to an overlap of 25 mm. In fact, a strength improvement of 99.3% was found with L_O raising from 12.5 to 25 mm. In addition, it was found a Pm variation of 7.12% with L_O ranging from 25 to 37.5 mm and -1.01% from 37.5 to 50 mm. Thus, it is important to refer that bigger L_O promote the inner adherend's failure and limit P_m to ≈24 kN.

4.2.2. Mixed-mode crack propagation criterion validation

Fig. 7 shows the comparison between the P_m values obtained experimentally with the numerical ones for the different L_O and α exponents for the SLJ (a) and DLJ (b) bonded with the Araldite® 2015. The pure-mode CZM laws of the adhesives were inserted by the definition of E, G_{xy}, t_n^0, t_s^0, G_{IC} and G_{IIC}. These properties were all taken from the data of Table 1, with the particularity that t_n^0 and t_s^0 are made equal to σ_f and τ_f, respectively (Campilho et al. 2011). The mixed-mode behaviour is defined from the damage initiation criterion (quadratic stress criterion in this case) and damage growth criterion (power law criterion with the user specification of α). The results showed that, for the SLJ, the most suitable α is 0.5, as predicted in the formerly discussed fracture tests, and that it gives a good representation of the experimental behaviour (as depicted in Fig. 5). The predicted P_m are always above the experiments, with relative differences that range between 4.9% (L_O=37.5 mm) to 14.4 (L_O=12.5 mm). This enables validating the mixed-mode criterion for crack propagation. On the other hand, the other tested α revealed higher deviations by increasing α up to a value of 2. Here, the maximum offset was 40.7%, for L_O=50 mm. An identical agreement was also found for the DLJ. However, for L_O≥25 mm, the joints' failure becomes governed by the net adherends' fracture, and the P_m results between different α become insignificant. Also because of this, the deviations are generally not relevant. For α=0.5, the maximum error was -3.5% for L_O=50 mm. Between all α, the maximum error was +5.5% (α=2 and L_O=25 mm). As a result of this discussion, the formerly obtained experimental envelope is validated. In addition, the slight deviations between the experiments and simulations were found to due to using a triangular CZM to model a highly ductile adhesive (Kafkalidis and Thouless 2002).

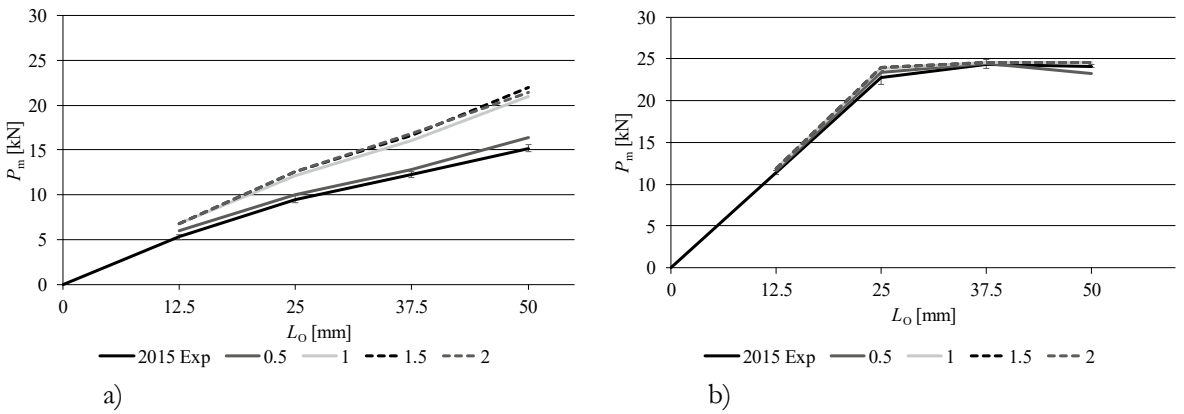

Fig. 7. Comparison between experimental and numerical P_m values for the SLJ (a) and DLJ (b) considering different α.

5. Conclusions

The proposed work aimed at experimentally defining the most suitable α parameter for the mixed-mode crack propagation prediction of a ductile adhesives. With this purpose, pure and mixed-mode fracture tests were undertaken that enabled building the fracture envelopes of the Araldite® 2015. This adhesive revealed a ductile failure, which, together with the G_I/G_{II} and G_{IC}/G_{IIC} values obtained, confirmed the expected ductile behaviour. The *R*-curves enabled estimating the data points that were on the basis of the built fracture envelopes. The experimental data points revealed

a different mixed-mode behaviour, with α=0.5 giving a close match. Validation of this data was undertaken with SLJ and DLJ. However, a previous experimental data discussion was presented, enabling to realize that for these geometries, less strong but ductile adhesives take advantage, on view of the ability to endure loads after damage onset takes place. After this analysis, numerical simulations of the SLJ and DLJ were made with different α, and P_m was compared with experiments. The energetic criterion resulting from the experimental work provided matching numerical results and, thus, the fracture envelopes were validated. In the end, this work made possible, by CZM, to estimate the most suitable α parameter to use in crack propagation of adhesive joints under mixed-mode conditions.

References

Abaqus® (2013). Documentation of the software Abaqus®. Dassault Systèmes. Vélizy-Villacoublay

Adams, R. D. (2005). Adhesive bonding: science, technology and applications. Cambridge, Woodhead Publishing Limited.

Barenblatt, G. I., 1959. The formation of equilibrium cracks during brittle fracture. General ideas and hypotheses. Axially-symmetric cracks. Journal of Applied Mathematics and Mechanics 23(3), 622-636.

Campilho, R. D. S. G., Banea, M. D., Neto, J. A. B. P. and da Silva, L. F. M., 2013. Modelling adhesive joints with cohesive zone models: effect of the cohesive law shape of the adhesive layer. International Journal of Adhesion and Adhesives 44, 48-56.

Campilho, R. D. S. G., Banea, M. D., Pinto, A. M. G., da Silva, L. F. M. and de Jesus, A. M. P., 2011. Strength prediction of single- and double-lap joints by standard and extended finite element modelling. International Journal of Adhesion and Adhesives 31(5), 363-372.

Choupani, N., 2008. Mixed-mode cohesive fracture of adhesive joints: Experimental and numerical studies. Engineering Fracture Mechanics 75(15), 4363-4382.

Constante, C. J., Campilho, R. D. S. G. and Moura, D. C., 2015. Tensile fracture characterization of adhesive joints by standard and optical techniques. Engineering Fracture Mechanics 136, 292-304.

da Silva, J. F. M. G., Öchsner, A. and Adams, R. D. (2011). Handbook of Adhesion Technology. Heidelberg, Springer.

de Moura, M. F. S. F., Campilho, R. D. S. G. and Gonçalves, J. P. M., 2009. Pure mode II fracture characterization of composite bonded joints. International Journal of Solids and Structures 46(6), 1589-1595.

Dugdale, D. S., 1960. Yielding of steel sheets containing slits. Journal of the Mechanics and Physics of Solids 8(2), 100-104.

Feraren, P. and Jensen, H. M., 2004. Cohesive zone modelling of interface fracture near flaws in adhesive joints. Engineering Fracture Mechanics 71(15), 2125-2142.

He, X., 2011. A review of finite element analysis of adhesively bonded joints. International Journal of Adhesion and Adhesives 31(4), 248-264.

Kafkalidis, M. S. and Thouless, M. D., 2002. The effects of geometry and material properties on the fracture of single lap-shear joints. International Journal of Solids and Structures 39(17), 4367-4383.

Moreira, R. D. F. and Campilho, R. D. S. G., 2015. Strength improvement of adhesively-bonded scarf repairs in aluminium structures with external reinforcements. Engineering Structures 101, 99-110.

Nunes, F. A. A. and Campilho, R. D. S. G., 2018. Mixed-mode fracture analysis of adhesively-bonded joints using the ATDCB test specimen. International Journal of Adhesion and Adhesives 85, 58-68.

Pardoen, T., Ferracin, T., Landis, C. M. and Delannay, F., 2005. Constraint effects in adhesive joint fracture. Journal of the Mechanics and Physics of Solids 53(9), 1951-1983.

Petrie, E. W. (1999). Handbook of adhesives and sealants. New York, McGraw-Hill.

Ribeiro, T. E. A., Campilho, R. D. S. G., da Silva, L. F. M. and Goglio, L., 2016. Damage analysis of composite–aluminium adhesively-bonded single-lap joints. Composite Structures 136, 25-33.

Rocha, R. J. B. and Campilho, R. D. S. G., 2018. Evaluation of different modelling conditions in the cohesive zone analysis of single-lap bonded joints. The Journal of Adhesion 94(7), 562-582.

Rodrigues, T. A. F., Chaves, F. J. P., Silva, L. F. M. d., Costa, M. and Barbosa, A. Q., 2017. Determination of the fracture envelope of an adhesive joint as a function of moisture. Materialwissenschaft und Werkstofftechnik 48(11), 1181-1190.

Sistaninia, M. and Sistaninia, M., 2015. Theoretical and experimental investigations on the mode II fracture toughness of brittle materials. International Journal of Mechanical Sciences 98, 1-13.

Szekrényes, A. and Uj, J., 2004. Beam and finite element analysis of quasi-unidirectional composite SLB and ELS specimens. Composites Science and Technology 64(15), 2393-2406.